Heliyon 11 (2025) e41414

Contents lists available at ScienceDirect

Heliyon

journal homepage: www.cell.com/heliyon

Research article

Extracellular domain of TREM2 possess two distinct ligand recognition sites: Insights from machine-learning guided docking and all-atoms molecular dynamics simulations

Sarbani Mishra [a], Preety Sthutika Swain [a], Sanghamitra Pati [a,**], Budheswar Dehury [b,*]

[a] ICMR-regional Medical Research Centre, Nalco Square, Chandrasekharpur, Bhubaneswar, 751023, Odisha, India
[b] Department of Bioinformatics, Manipal School of Life Sciences, Manipal Academy of Higher Education, Manipal, India

ARTICLE INFO

Keywords:
Neurodegenerative disorders
TREM2 ECD
AD
NHD
Complementarity-determining regions
Mutation

ABSTRACT

The myeloid-specific triggering receptors expressed on myeloid cells 2 (TREM2) is a group of class I receptors expressed in brain microglia plays a decisive role in neurodegenerative diseases such as Alzheimer's disease (AD) and Nasu Hakola disease (NHD). The extracellular domain (ECD) of TREM2 interacts with a wide-range of ligands, yet the molecular mechanism underlying recognition of such ligands to this class I receptor remains underexplored. Herein, we undertook a systematic investigation for exploring the mode of ligand recognition in immunoglobulin-like ectodomain by employing both knowledge-based and machine-learning guided molecular docking approach followed by the state-of-the-art all atoms molecular dynamics (MD) simulations. Besides the known binding site formed by complementarity-determining regions (CDR) 1 and CDR2 loops, which enables the binding of different anionic ligands, our study identifies the presence of second binding site formed by β-strands towards the C-terminal end. We observe a dense network of hydrophobic contacts formed between the explored ligands and CDR loops and β-strands, specifically CDR1, CDR2, β-strand C', loop connecting β-strand D and E, and loop connecting β-strand E and F. Ligand binding in immunoglobulin-like ectodomain increases the conformational flexibility of CDR2 loop, thus most frequently observed pathogenic variants i.e. R47H and R62H in TREM2 may affect the development and progression of AD. Our knowledge-based and machine-learning guided docking and physics-based simulations study unveils deep insights into the endogenous ligand recognition by the positive surface ligand binding site and distant core site pave the way for exploration of other small molecules towards development of novel therapeutics against Alzheimer's disease.

1. Introduction

Triggering receptors expressed on myeloid cells 2, TREM2, are a group of immune receptors expressed by mononucleolar phagocytes including alveolar macrophages, microglia and osteoclasts on the cell surface and intracellular pools of the central nervous

* Corresponding author.
** Corresponding author.drsanghamitra12@gmail.com
E-mail address: budheswar.dehury@manipl.edu (B. Dehury).

https://doi.org/10.1016/j.heliyon.2024.e41414
Received 17 June 2024; Received in revised form 19 December 2024; Accepted 20 December 2024
Available online 20 December 2024

system, bone, liver, adipose tissue, skin, gut and tumours. TREM2 comprises of a single extracellular V-type immunoglobulin domain positioned on a flexible stalk in the extracellular region connected via β-sheet G, a transmembrane domain and a short intracellular cytoplasmic tail at the C-terminus [1–4]. A wide array of functions encompassing cell maturation, survival, proliferation, activation, phagocytosis, lipid processing, lysosomal degradation and regulating inflammation have been associated to TREM2 [5]. Furthermore, a diverse range of neurodegenerative diseases including Alzheimer's disease (AD), frontotemporal dementia (FTD), Nasu-Hakola disease (NHD), and Parkinson's disease (PD) have been linked to the loss of function of the receptor as an outcome of homozygous and heterozygous mutation [6–10]. Genetic studies have successfully shown the critical role of TREM2 in amyloid plaque compaction in AD and its slower progression [6,7].

Protein-ligand interactions, responsible for signal transmission, immune response, and gene regulation are crucial for offering a theoretical framework for developing and identifying new therapeutic targets [11] associated with neurodegenerative diseases. Though the endogenous ligands of TREM2 are yet to be unveiled, experimental studies have shown its acknowledgement towards phospholipids, apoptotic cells, and lipoproteins [12–15]. Wide range of anionic molecules, bacterial products, and DNA are also considered as active TREM2 ligands [16]. Putative ligands like apolipoprotein E (apoE) and apolipoprotein J (apoJ) have been reported to show higher affinity towards TREM2 upon activation due to anionic lipid binding [12–15]. The unrestrained character of this class of receptor is consistent with its capacity to engage with a variety of endogenous and substitute ligands in diverse physiological and challenging settings by possibly engaging various molecular interaction surfaces [17].

TREM2 signalling is specifically dependent on immunoreceptor tyrosine-based activating motif (ITAM) i.e., DAP12 and DAP10, which acts by phosphorylating proteins phosphatidylinositol 3-kinase (PI3-K) and protein tyrosine kinase Syk for pathway activation respectively [18]. Additionally, ADAM10/17 regulates the function of TREM2 through intracellular trafficking and proteolytic cleavage of the ligand binding ectodomain [19,20]. These phosphorylated co-receptors activate the intracellular signalling apparatus upon exposure to TREM2-ligands.

The broad array of TREM2 ligands makes it difficult to predict the outcomes of their binding, and the range of ligands are a result of tissue damage and cell death [16,21,22]. TREM2 extracellular domain (ECD) binds to Phosphatidylserine (PS), phosphatidylethanolamine (PE), Phosphatidylcholine (PC), and sulfo-glucolipid [14,22,23]. TREM2-expressing cells readily remove ligands such as phosphatidylserine, presenting cellular debris or sulfatide, covered with myelin debris, pointing towards the involvement of TREM2 in the initial stage of phagocytic clearance [15,24,25]. Sphingnosinde-1-phosphate (S1P), another TREM2 ligand that encourages microglial phagocytosis to guard against ischemic brain damage [26] are bioactive lipids generated by the phosphorylation of sphingosine, a sphingolipid metabolite [27]. Sometimes they might act as a microglial phagocytosis regulator as well as a switch from homeostatic to disease associated microglia state [28,29]. However, AD risk enhancing TREM2 variants R47H and R62H are found to be associated with the impaired binding of phospholipids [12,13,30].

TREM2 is also actively regulated by ectodomain shedding of the ECD by a disintegrin and metalloproteinase domain-containing protein 10 (ADAM10) followed by intramembranous cleavage of the remaining C-terminal transmembrane domain and intracellular domain by γ-secretase [19,31]. sTREM2, produced by cleavage of TREM2 ectodomain or by alternative splicing, possess ligand binding capacity and decreases Aβ plaques in AD brain, and also serves as a biomarker that regulates the immune response in AD [32]. Additionally, post-transcriptional modifications in the ECD including glycosylation or sulfidation may influence TREM2 functioning [33]. Moreover, the highly conserved nature of TREM2 ECD, as demonstrated in Fig. 1, highlights its significance in regulating various essential biological processes. For this reason, it is very important to understand the structural intricacies of TREM2 ECD to achieve insights into any ligand induced significant structural changes, which might in return affect the fundamental cellular functions. Therefore, we have directed our focus on the computational-biophysical and structural study of ligand bound TREM2 ECD utilizing knowledge-based and machine-learning guided molecular docking and state-of-the-art all-atoms molecular dynamics (MD) simulations (Fig. 1), critical for understanding the conformational shift of proteins brought on by ligand binding [34]. Our findings

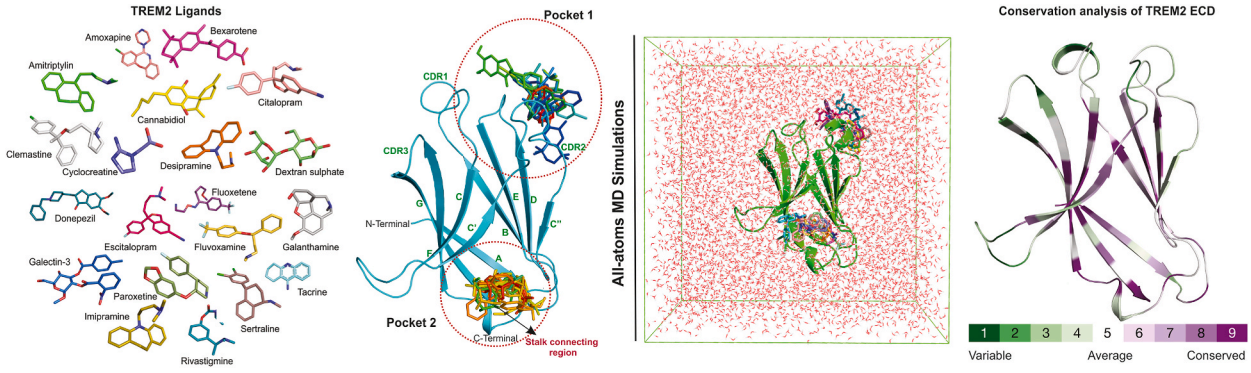

Fig. 1. Schematic representation of TREM2 ECD-ligand interaction. Left panel highlights the three-dimensional structures of selected ligands used in the current study. Middle left panel highlights the docked conformation of TREM2 ECD-ligands that was performed through both knowledge based and machine learning guided molecular docking. Middle right panel demonstrates a MD simulation box with docked TREM2 ECD-ligand complexes. Right panel highlights the conservation profile of TREM2 ECD analysed through ConSurf, where green colour indicates variable regions, and violet indicates conserved regions.

demonstrate the differential mode of ligand binding in the TREM2 ECD and presence of a new probable binding site. The insights attained from our study opens up new avenues to develop new effective therapeutics against neurological disorders targeting TREM2 ECD.

2. Materials and methods

2.1. Targeted protein and ligand assortment

In the current investigation on mode of interaction between TREM2 ECD and its ligands and the effect of small molecules in the structure of TREM2 ECD, we have used the crystalized structure of TREM2 ECD (PDB ID: 6B8O) bound to Phosphatidylserine was retrieved from RCSB PDB [35]. We extracted one protomer of ECD from the retrieved structure and processed it for further analyses. There are existing studies that vividly investigates the interaction between TREM2 and its endogenous ligands [15,16]. However, scant knowledge is available regarding the structural information of TREM2 upon interaction with small molecules such as antidepressants, cannabis and drugs specific for AD. Therefore, we chose twenty TREM2 ligands with diverse range of chemical structures available from literature to understand their possible interactions. Proposed molecules from the literature were fetched in their 3D conformations from PubChem database [36] in SDF format for further analyses. Molecules, whose structure were absent in the database were drawn using ChemSketch [37]. All the retrieved molecules were then assembled and prepared for molecular docking interaction studies.

2.2. Structure preparation of TREM2 ECD and its ligand, grid box generation

The foremost essential step in molecular docking is preparation of the target protein and ligands. Refinement of TREM2 ECD was carried out using AutoDockTools, with deletion of water molecules and heteroatoms along with addition of polar hydrogen atoms and Kollman's charge. The optimized protein structure was then exported in ".pdbqt" format to perform molecular docking studies. After confirming ligands, they were converted into AutoDock Vina [38] readable format (.pdbqt) using Open Babel tool [39]. For generation of the grid, we retrieved the already known information regarding the active site of TREM2 ECD from the literature, while state-of-the-art machine learning mediated PrankWeb tool provided us information regarding the coordinates of a new binding site. In the subsequent step the grid box was generated with a grid dimension of $52 \times 52 \times 52$ and 0.375 Å grid spacing for docking analysis. The exhaustiveness for performing molecular docking was set to 8 and finally a total of 10 modes were generated for each TREM2 ECD-ligand complex.

2.3. Determination of TREM2 ECD-ligand poses using molecular docking

To perform molecular docking, we chose AutoDock Vina docking program because of its free availability, proven accuracy and programming efficiency in the field of academic research [40,41]. We determined the binding affinities and mode of TREM2 ECD-ligand binding through the knowledge-based scoring function implemented in AutoDock Vina. The empirical information available in the docking program was then used to rank the ten docked conformations, based on their binding affinities. The protocol and accuracy for AutoDock Vina have also been validated in our previous studies [42,43]. TREM2 ECD-ligand poses that displayed higher binding affinity were selected as best docked conformers due to their stronger and energetically favourable interactions suggesting towards higher stability amongst all the docked poses and hence, were chosen for further analyses. All the docked conformations were visualized using BIOVIA Discovery Studio Visualizer. To confirm their structural orientation and integrity of TREM2 ECD-ligand complexes, classical all-atoms MD simulations were performed in aqueous solution.

2.4. TREM2 ECD-ligand system setup and molecular dynamics simulation

TREM2 ECD-ligand docked complex structures were then processed using the structure-based balanced CHARMM36m [44] and CHARMM General Force Field (CGenFF) [45] for the protein and ligand structures respectively, in TIP3P water model in GROMACS *v*2020. Periodic boundary conditions were used for all the protein-ligand complexes. To electro-neutralize the protein-ligand-water complex system, 0.15 M NaCl counter ions were added. Following the process of neutralization, each system was subjected to energy minimization to obtain a geometrically reasonable starting structure and a two-phase equilibration process was also performed using isothermal-isochoric NVT and isothermal-isobaric NPT ensemble. Energy minimization was carried out using the steepest descent optimization for 5000 steps. On the other hand, the complex systems underwent the two-phase equilibration for 100 ps at 310.15K each for both NVT and NPT ensembles using the Parrinello-Rahman method [46] and Nose-Hoover thermostat [47] respectively. Finally, a production MD of 200 ns was run at 1 bar and 310.15K for each complex system. The long-range electrostatic interactions were calculated using the standard particle mesh Ewald method [48], while the cut-off for short-range electrostatic and van der Waals forces was set in the range of 10–12 Å. All the hydrogen bonds were restrained using the SHAKE algorithm [49]. The current protocol for MD simulation was adapted from previous studies described elsewhere [50,51]. To further have a comparative illustration of the effect of ligand binding on the structural features of TREM2 ECD, we also performed a MD simulation on the apo wild type structure (PDB ID: 5UD7) and R47H mutant (5UD8) with same parameters as mentioned above.

2.5. Computational analysis of the MD trajectories

To acquire the dynamics stability in each TREM2-ECD apo wild type, R47H (mutant) and ligand-bound TREM2 complexes, and evaluate the conformational changes and effect of ligand binding on the structure of TREM2 ECD, we calculated their backbone RMSD, radius of gyration (Rg), C-alpha root mean square fluctuations (RMSF), and solvent accessible surface area using *gmx rms, gmx gyrate, gmx rmsf* and *gmx sasa* GROMACS analysis toolkit. Inter-molecular hydrogen bonds between the interacting TREM2 ECD residues and

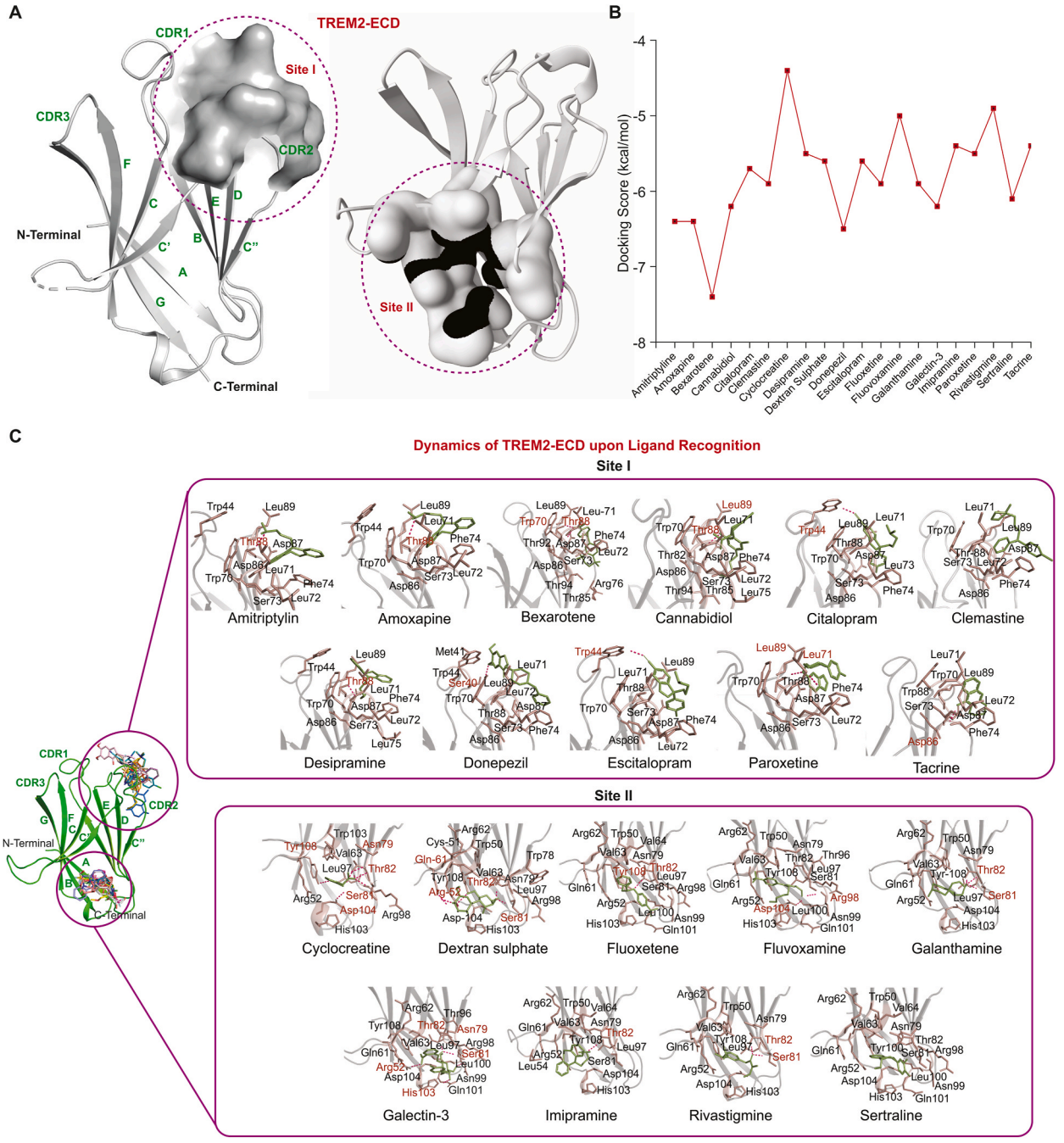

Fig. 2. Ligand binding sites and molecular docking assessment of TREM2 ECD and its known ligands. (**A**) Two different ligand binding site, site I and site II in TREM2 ECD. Both the binding sites have been shown in surface representation. (**B**) Line graph demonstrating the trend of binding energy of each TREM2 ligand against TREM2 ECD assessed through molecular docking. (**C**) Intermolecular contacts of formed between each TREM2 ECD-ligand docked complexes. Ligand interacting residues have been shown in stick, while TREM2 ECD has been demonstrated in cartoon. Hydrogen bond forming residues have been highlighted in red and hydrogen bonds are shown in red dotted lines.

Table 1
Ensembled list of compounds used in the study with their docking score and amino acids associated in forming non-bonded interactions with TREM2 ECD.

Site I					
Sl. No	PubChem ID	Complex	Docking score (kCal/mol)	H-bond	Hydrophobic contacts
1	2160	Amitriptyline	−6.4	Thr88	Trp44, Trp70, Leu71, Leu72, Ser73,Phe75,Asp86, Asp87,Leu89
2	2170	Amoxapine	−6.4	Thr88	Trp44, Trp70,Leu71,Leu72,Ser73,Phe74,Asp86, Asp87,Leu89
3	82146	Bexarotene	−7.4	Thr88	Trp70,Leu71,Leu72,Ser73,Phe74,Leu75,Arg76,Thr85,Asp86,Asp87,Leu89, Thr92,Thr94
4	644019	Cannabidiol	−6.2	Thr88, Leu89	Trp70, Leu71, Leu72, Ser73, Phe74, Leu75, Thr85, Asp86, Asp87, Thr92
5	2771	Citalopram	−5.7	Trp44	Trp70, Leu71, Leu72, Ser73, Phe74, Asp86, Asp87, Thr88, Leu89
6	26987	Clemastine	−5.9		Trp44,Trp70,Leu71,Leu72,Ser73,Phe74,Asp86,Asp87,Thr88,Leu89
7	2995	Desipramine	−5.5	Thr88	Trp44,Trp70,Leu71,Leu72,Ser73,Phe74,Leu75, Asp86,Asp87,Leu89
8	3152	Donepezil	−6.5	Ser40, Trp44	Met41, Trp44, Trp70, Leu71, Leu72, Ser73, Phe74, Asp86, Asp87, Thr88, Leu89
9	146570	Escitalopram	−5.6	Trp44	Trp70, Leu71, Leu72, Ser73, Phe74, Asp86, Asp87, Thr88, Leu89
10	43815	Paroxetine	−5.5	Leu89, Leu71	Trp70, Leu72, Ser73, Phe74, Asp86, Asp87, Thr88
11	1935	Tacrine	−5.4	Asp86	Trp70, Leu71, Leu72, Ser73, Phe74, Asp87, Thr88, Arg98
Sl. No	**PubChem ID**	**Complex**	**Docking score (kCal/mol)**	**H-bond**	**Hydrophobic contacts**
1	2896	Cyclocretine	−4.4	Ser81, Asp104, Thr82	Trp50, Arg52, Val63, Asn79, Leu97, Arg98, His103, Tyr108
2	129675657	Diethylaminoethyl_dextran	−5.6	Arg52, Ser81, Gln61, Thr82	Trp50, Cys51, Arg62, Val63, Asn79, Leu97, Arg98, His103, Asp104, Tyr108
3	3386	Fluoxetine	−5.9	Ser81, Thr82, His103, Tyr108	Trp50, Arg52, Gln61, Arg62, Val63, Asn79, Ser81, Leu97, Arg98, Asn99, Leu100, Gln101, His103, Asp104
4	5324346	Fluvoxamine	−5	Arg98, Asp104	Trp50, Arg52, Gln61, Arg62, Val63, Asn79, Ser81, Thr82, Thr96, Leu97, Asn99, Leu100, Gln101, His103, Tyr108
5	9651	Galanthamine	−5.9	Thr82, Ser81	Trp50, Arg52, Gln61, Arg62, Val63, Asn79, Leu97, Asp104, His103, Tyr108
6	163409169	Galectin-3	−6.2	Arg52, Ser81, Thr82, His103	Gln61, Arg62, Val63, Asn79, Thr96, Leu97, Arg98, Asn99, Leu100, Gln101, Asp104, Tyr108
7	3696	Imipramine	−5.4	Thr82	Trp50, Arg52, Gln61, Arg62, Val63, Val64, Asn79, Ser81, Leu97, His103, Asp104, Tyr108
8	77991	Rivastigmine	−4.9	Ser81, Thr82	Trp50, Arg52, Gln61, Arg62, Val63, Asn79, Leu97, His103, Asp104, Tyr108
9	68617	Sertraline	−6.1		Trp50, Arg52, Gln61, Arg62, Val63, Asn79, Ser81, Thr82, Leu97, Arg98, Asn99, Leu100, Gln101, His103, Asp104, Tyr108

ligands of each system were explored with the help of *gmx hbond* toolkit. Evolutionary changes in the secondary structure profile of the protein during the 200 ns MD simulation were monitored using the timeline viewer of VMD.

2.6. Essential dynamics

The collective motions of each TREM2 ECD-ligand system was assessed from their local dynamics by condensing the datasets of larger motion into subset made up of principal components (PCs) [52]. Principal component analysis (PCA) on each TREM2 ECD-ligand complexes were performed using the *gmx anaeig* and *gmx covar* modules of GROMACS using the last 100 ns MD trajectories. A set of eigenvectors and eigenvalues expressing collective motion of the molecules for each complex was extracted by diagonalizing the covariance matrix.

2.7. Estimation of MM/PBSA binding free energy

Molecular-Mechanics Poisson-Boltzmann Surface area (MM/PBSA) is a method that determines the binding free energy of a system by using the initial conformation of the receptor and ligand as well as the conformation of the complex [53]. For the evaluation of binding free energy of each complex *g_mmpbsa* tool was considered. A total of 200 snapshots at equal time interval were extracted from the last 100 ns of each MD trajectory for the estimation of binding energy (ΔG_{bind}). The following equations were used for calculation of ΔG_{bind}:

$$\Delta G_{bind} = G_{Complex} - G_{Protein} - G_{Ligand} = \Delta E_{MM} + \Delta G_{sol} - T\Delta S \quad (1)$$

$$\Delta E_{MM} = \Delta E_{bonded} + \Delta E_{nonbonded} = \Delta E_{bonded} + (\Delta E_{vdw} + \Delta E_{ele}) \quad (2)$$

$$\Delta G_{sol} = \Delta G_{polar} + \Delta G_{nonpolar} \quad (3)$$

where, ΔE_{MM}, ΔG_{sol} and $T\Delta S$ illustrate energy contributions of molecular mechanics energy, solvation free energy and entropy upon ligand binding respectively. To comprehend the contribution of each amino acid towards the total binding energy, we performed per-residue energy decomposition analysis. The complete protocol for binding free energy decomposition analysis have been describe elsewhere [43,54].

3. Results and discussion

3.1. TREM2 ectodomain possesses multiple ligand binding sites

Earlier investigation on the immunomodulatory receptor, TREM2 has shown their involvement in AD progression either through rare pathogenic mutations or through its selective expression in the myeloid cells, promoting the optimal functioning of the microglia and regulating their energetic metabolism [6,55]. Binding of TREM2 and DAP12 within the cell membrane has been proposed to be critical for the initiation of TREM2 signalling pathway. The mechanism of TREM2 signalling is triggered by its differential binding to numerous ligands in the ECD, which in return activates the downstream pathway involving stable interaction between TREM2 and DAP10/12 [56]. Interaction of such ligands is significant to determine its differential signalling intensity and direction of TREM2 [16]. Molecular docking analysis performed in the current research work allows the behavioural characterization of such small molecules in

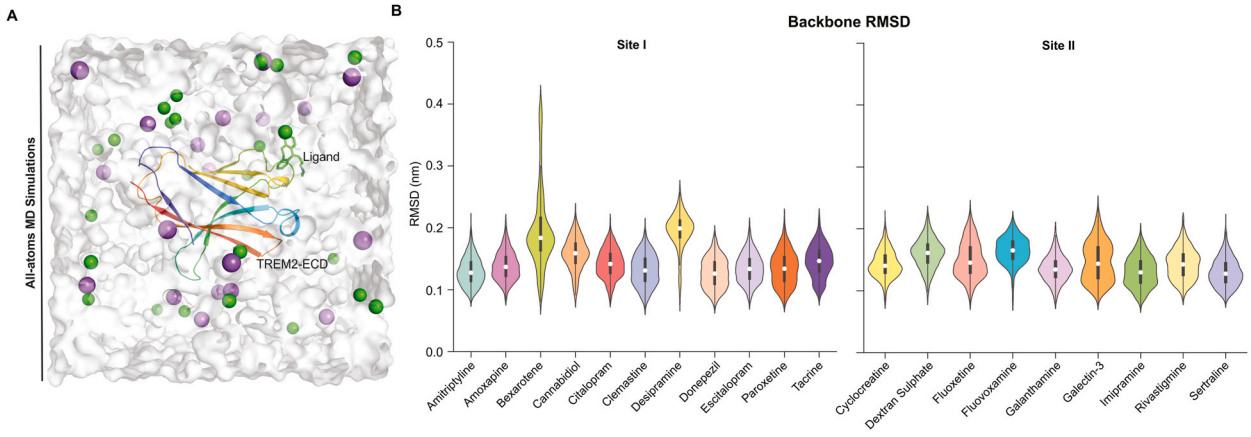

Fig. 3. Structural stability of TREM2 ECD upon binding to ligands assessed through MD simulations. (**A**) A snapshot of simulation box filled with TIP3P solvent electro-neutralized Na^+ and Cl^- ions, TREM2 ECD and a docked ligand (**B**) Backbone RMSD of MD simulated TREM2 ECD-ligand complexes represented in violin plots. Left panel indicates systems with ligands docked at site I of TREM2 ECD while right panel highlights the backbone RMSD of complexes with ligands docked in site II of TREM2 ECD.

the binding site of our target protein [57]. For molecular docking, we initially retrieved the coordinates of the known binding site i.e., site I in ECD from literature [58], while we also utilized PrankWeb, a state-of-the-art machine learning based ligand binding site prediction tool [59] to identify any other probable binding site. Surprisingly, PrankWeb identifies a second binding pocket in TREM2 ECD with highest probability (Fig. 2A and S1).

TREM2-ECD forms a β-sandwich comprising nine antiparallel β-strands labelled from A-G with additional C' and C" strands as per the Williams and Barkley conventions [60] and three CDR loops namely CDR1 (Pro^{37}-Arg^{47}), CDR2 (Thr^{66}-Arg^{76}), CDR3 (His^{144}--Glu^{117}) [61]. A close inspection of the docked poses of ligands within the binding pocket of TREM2 ECD illuminated us with the presence of two binding sites: one closer to the CDR loops, i.e., site I and another towards the beta strands nearby C-terminal end,

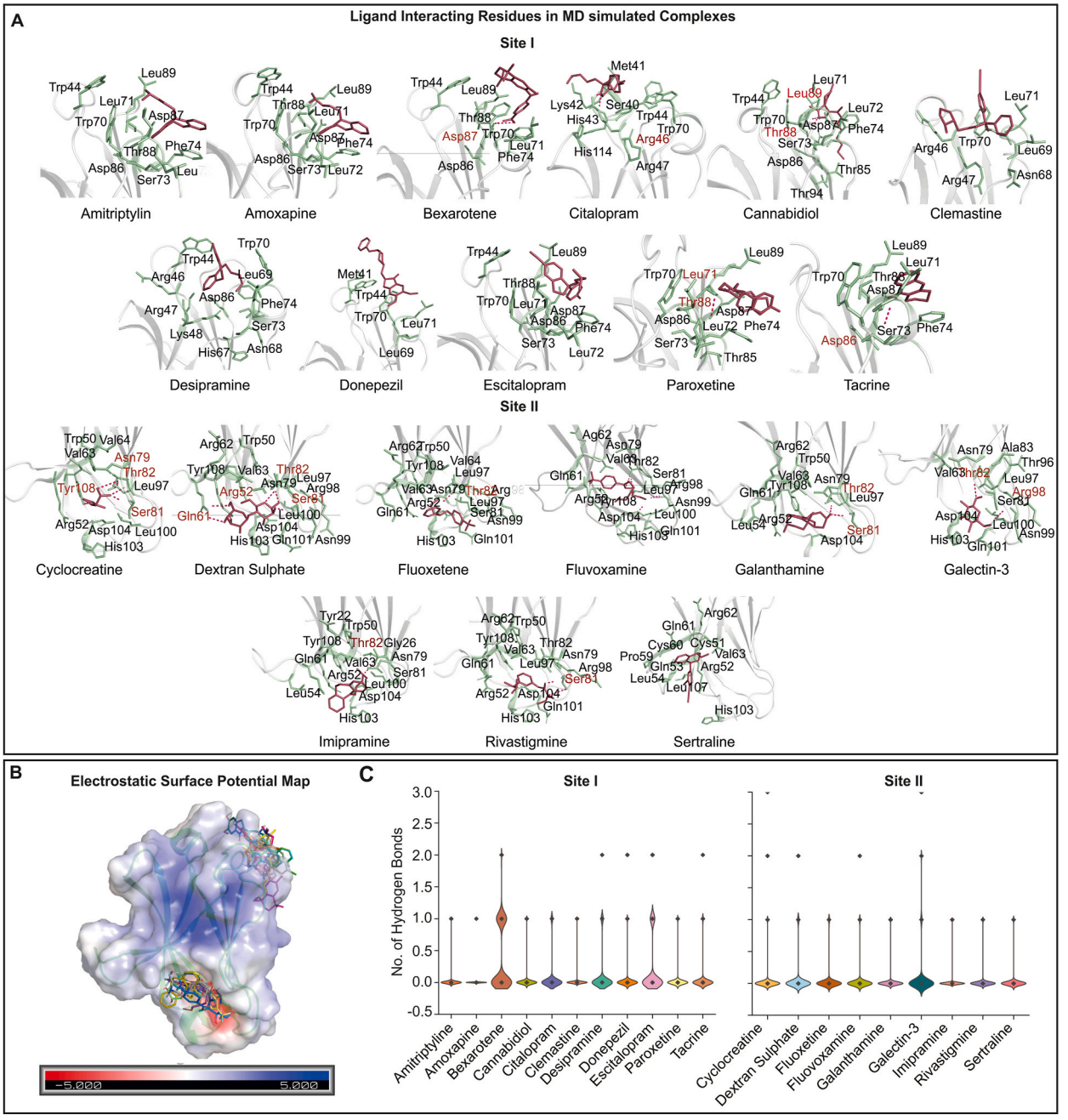

Fig. 4. Interaction pattern of TREM2 ECD and ligands along with their electrostatic surface potential map. (**A**) Intermolecular non-bonded interactions formed between MD simulated TREM2 ECD and ligands in their respective binding sites i.e., site I and site II. (**B**) Distribution of surface charges on the MD simulated ligand bound TREM2 ECD. (**C**) Number of intermolecular hydrogen bonds formed between TREM2 ECD and its ligands throughout the 200 ns timescale.

namely site II (Fig. 2A). The presence of multiple binding sites in TREM2 ECD has been confirmed by two independent studies [62,63]. Significantly, site II has been studied to be involved in binding apolipoproteins which has also been studied in our recent investigation [63,64]. Another recent research on biophysical mapping of TREM2-ligand interactions explores the structural intricacies of how TREM2 engages with various ligands [65]. This study also confirms the presence of our binding site I and II in TREM2 ECD and also highlights the importance of hydrophobic interactions in ligand binding. Notably, site I and II could be opted as therapeutic targets for

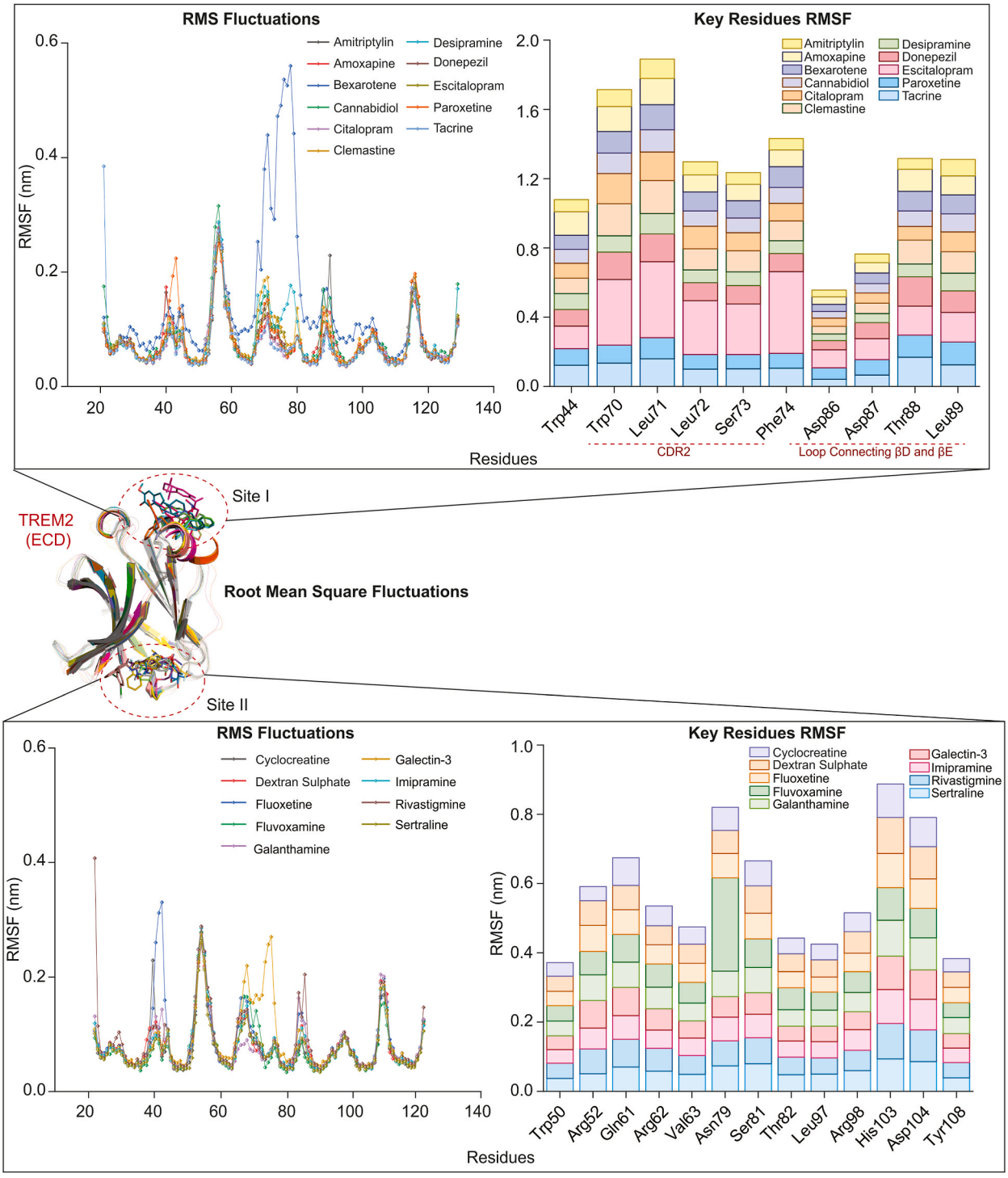

Fig. 5. Ligand induced changes on TREM2 ECD depending on the site of interaction assessed post MD simulations. Line plots represent the RMSF profile of the Cα atoms of whole TREM2 ECD. RMSF of key residues have been illustrated in the bar plots.

modulating TREM2-ligand interactions for modifying TREM2 function and microglia activities.

Interplay between TREM2-ECD and fetched 20 small molecules was assessed based on their binding affinity towards TREM2-ECD (Table 1). Based on their binding affinity, we noticed that Bexarotene possessed higher binding affinity, suggesting towards its most stable interaction with TREM2 ECD (Fig. 2B and Table 1). A vivid analysis of all 20 protein-ligand complexes highlighted the residues involved in forming intermolecular interactions with TREM2 ECD (Table 1).

Ligands interacting to the site I of TREM2 ECD exhibited active involvement with amino acids residues Trp44 (CDR1), Trp70, Leu71, Leu72, Ser73 and Phe74 from CDR2, Ser81 and Thr82 from β6 and, Thr88 from loop connecting β6 and β7 through a dense network of hydrophobic contacts (Table 1). On the other hand, Trp50 (β-strand C), Arg62 and Val63 from β-strand C', Ser81 and Thr82 from β-strand D, and His103 residue from loop connecting β-strand E and F of TREM2 ECD were found to be predominantly interacting with ligands in site II. Thr88 and Trp44 were seen to have dominant role in forming hydrogen bonds with the ligands in site I, whereas Ser81 and Thr82 from site II had maximum contribution in formation of polar contacts. A clear representation of non-bonded representation has been enumerated in Fig. 2C.

3.2. Structural stability of TREM2 ECD-ligand bound complexes

Recently, several researches have demonstrated the inability of microglia to eliminate supernumerary synapse during brain development, altered brain connectivity, behavioural defects, impaired neuronal transcriptomic and energetic profile in the absence of TREM2 [23,66,67]. Moreover, there exists several lines of evidence, which suggest that homeostatic microglia exclusively rely on OXPHOS for ATP production, while inflammatory microglia undergo aerobic glycolysis for the same [68–70]. Having said that, enhanced expression of TREM2 is required for modulating cellular biosynthetic metabolism and inducing transcriptomic and functional DAM [56] and differentiate the transition of stage 1 to stage 2 DAM [71]. What is the mechanism underlying TREM2 activation? How does TREM2 behaves upon binding to ligands? How do TREM2 activation promotes phenotypic transition of stage 1 and stage 2 DAM? The proper functionality of TREM2 and its precise effect of activation in AD progression is still a matter of debate. While a group of researchers stick to the known functionality of TREM2 that promotes the clearance of amyloid β and suggests the development of therapeutic approaches focusing on enhancing TREM2 activity [72–74], there exists several researches which focuses on its inhibition [75]. Dysfunction of TREM2, caused due to reduced expression and mutations can be a major cause of AD progression by regulating neuroinflammation and immune response in brain. This dysfunction can also contribute to overproduction of proinflammatory cytokines, thus exacerbating inflammations. Therefore, there has been a constant discussion among researchers that inhibition of TREM2 can be an ideal approach to reduce inflammatory response in the brain, decrease neuroinflammation and eventually slowing down AD progression, however, the implications of this complex strategy requires further critical investigations. A detailed study on the structure of TREM2 and its mode of interaction with its ligands can aid in achieving a better understanding of TREM2 mechanism.

Therefore, our MD study can assist the development of drugs targeting TREM2 ECD through analysing its structural behaviour upon binding to different ligands. A simulation box consisting of water molecules, TREM2 ECD bound to a ligand and NaCl ions have been illustrated in Fig. 3A. Structural stability of all the TREM2 ECD-ligand complexes from both the groups were studied based on their backbone RMSD (Fig. 3B). Moreover, we also calculated the atomic deviation of ligands from their starting structure through calculation of ligand RMSD, as demonstrated in Fig. S2. As can be evident from Fig. 3B and Table S1, the RMSD of all the complexes ranges between ~0.13–0.19 nm. However, we observe a diverse range of deviation in case of ligand RMSD. This deviation in RMSD of ligands within the binding pocket of TREM2 ECD might have been resulted due to their change in orientation during the 200 ns MD simulation. Structural stability of our TREM2 ECD-ligand complexes can also be confirmed from their Rg and SASA profiles (Figs. S3 and S4 and Table S1).While compactness of each TREM2 ECD-ligand complex was assessed through their gyradius profile, evaluation of SASA provided us information regarding the area of TREM2 ECD exposed to solvent in each complex, with an observation of disruption in the compactness of bexarotene bound TREM2 ECD towards the end of simulation can be evident from Fig. S4 [76,77]. As can be evident from Table S1, Rg of each complex system ranges between ~1.37–1.39 nm, while SASA ranges between ~67 and 69 nm^2. When compared with the stability profile of both apo wild type and R47H mutant of TREM2 ECD structure, we observe similar behaviour of TREM2 ECD bound to ligands in reference to R47H mutant, while a more stable structure was evident in the apo structure (Fig. S5).

3.3. Hydrophobic contacts anchor the ligand within TREM2 ECD

As mentioned before, early studies have shown the bidirectional activity of TREM2 in both modulating phagocytosis, proliferation, inflammatory responses and lipid metabolism of microglia and development and progression of AD. Therefore, understanding the kind of molecular interactions between TREM2 and its ligands can aid in understanding its proper functionality. 2013 reports on heterozygous point mutations in TREM2, more specifically R47H identifies a three-fold increase in AD risk [6,55], while another study highlights that R47H mutation in TREM2 promotes inflammation, causes synapse loss and basic microglia functioning impairment [78]. Recently, a study by Sudom et al. on the wild type (WT) and R47H variant of TREM2 reveals the critical role of Arg47 in maintaining the structural stability of the N-terminal fold and region near the CDR 2 loop through a network of hydrogen bonds with Ser65, Thr66, His67 and Asn68, which was further strengthened by another set of hydrogen bonds formed between carbonyl and amide groups of Lys48 and Thr66 in the WT [62]. Additionally, homozygous loss-of-function T66M mutations have been studied to prevent TREM2 glycosylation and cell surface expression, thus causing polycystic lipomembranous osteodysplasia with sclerosing leukoencyphalopathy (PLOSL) and a frontotemporal dementia-like syndrome [31,79]. Furthermore, Kober and co-workers along with Sudom et al. shows that our ligand binding site I is also a phospholipid binding site which engages a hydrophobic patch and may also

act as a major binding site for ApoE [62,63]. On the other hand, Kober et al. also reveals the presence of another binding site in TREM2 ECD with a basic patch, which might be critical for the binding of anionic ligands like proteoglycans [63]. In the light of these findings, our extensive computational approach, for the first time, shows the possibility of presence of another potential site for the binding of small molecules.

Our intermolecular contact analysis of snapshots derived from MD reveals that most of the intermolecular interactions between TREM2 ECD and its ligands in both the sites were dominated by a dense network of hydrophobic interactions (Table S2). In case of site I binding ligands, we observed that Trp44 (CDR1 loop), Trp70, Leu71 and Phe74 from CDR2 loop, Thr88 and Leu89 from loop connecting β-strand D and E were observed in forming hydrophobic contacts with most of the ligands, while Thr44 was seen to predominantly form hydrogen bonds. On the other hand, we observed Arg52 (β-strand C), Arg62 (β-strand C'), Thr82 (β-strand D), Thr88 and Leu89 from loop connecting β-strand E and F, His103 and Asp10 from loop connecting -strand E and F, and Tyr108 (β-strand F) forming a dense network of hydrophobic contacts in case of site II while Ser81 was involved in forming polar contacts. Most importantly, we observed that Trp44, Thr88, Trp70, Leu71, Phe74 and Leu89 from site I and Arg52, Arg62, Val63, Thr82, His103 and Tyr108 residues from site II are preserved in both docking and MD studies (Figs. 4A and 2C). Hence, we can hypothesize that these residues might be playing significant role in the process of ligand recognition. However, further experimental validations are required for confirmation of their role.

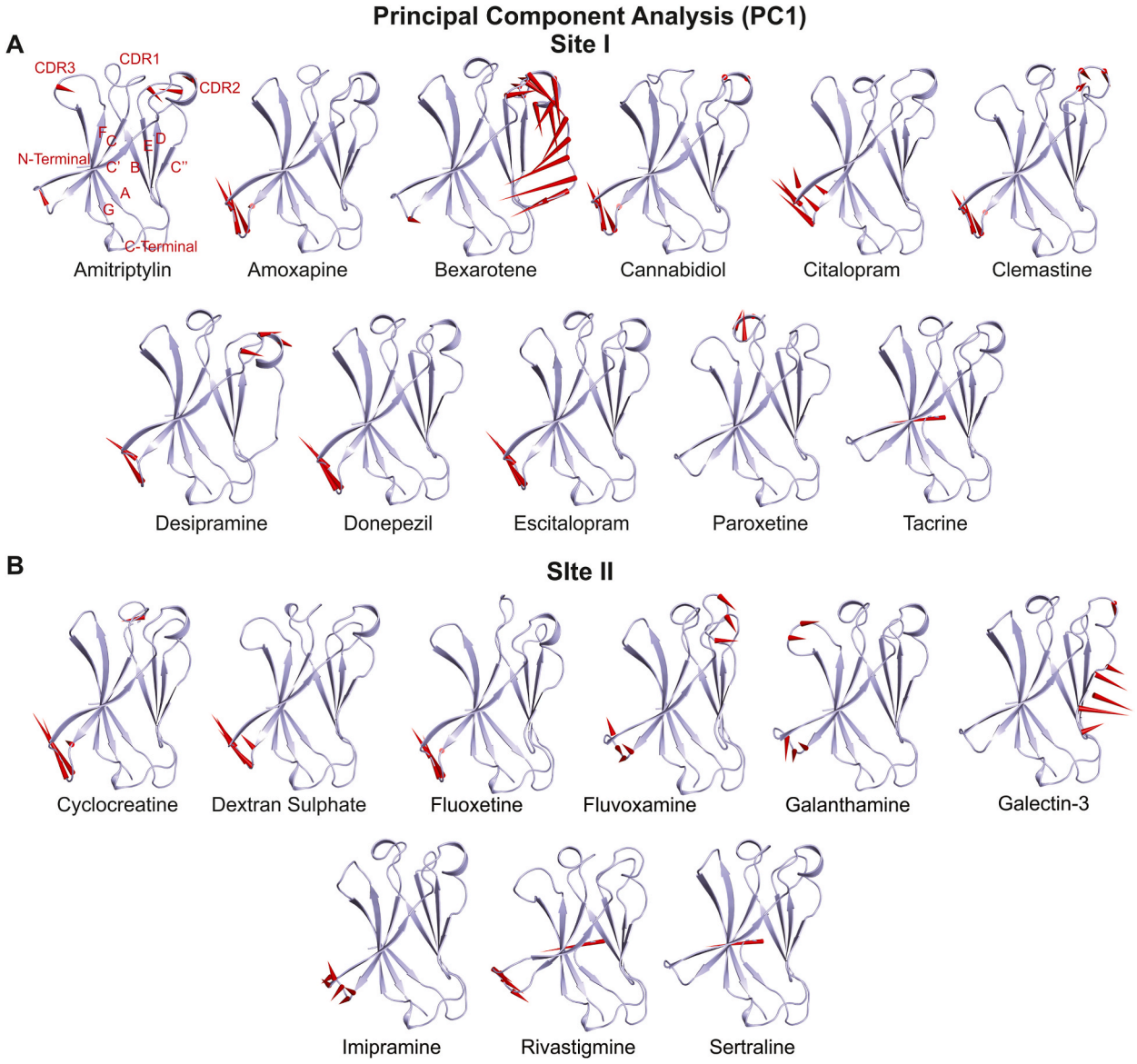

Fig. 6. Essential dynamics assessment of MD simulated TREM2 ECD upon ligand binding. (**A**) Porcupine plots of the mainchain atoms of the first PC of complexes with ligands bound at site I. (**B**) PC1 porcupine plots of the TREM2 ECD mainchain atoms from site II bound ligand complexes.

The electrostatic surface potential map of the MD simulated TREM2 ECD also highlights that the ligand binding site I is surfaced with mildly positively charged residues, while site II possesses negatively charged residues on the surface of the binding site (Fig. 4B). The electrostatic surface potential map was generated using the top MD simulated clusters of each TREM2-ligand complex through the APBS plugin implemented in PyMOL. To calculate the electrostatic surface potentials, we employed the default ion concentration of 0.15 M with dielectric constant of 2 and 78 for protein and solvent respectively at 298 K. Approximately, similar distribution of the surface charges were observed in the WT TREM2 ECD [62]. The discrepancies in intermolecular interactions and the surface charge distribution of TREM2-ligand complexes might have been a result of ligand induced conformational changes in TREM2 or chemical properties of the ligands. The complexity of intermolecular contacts in TREM2-ligand complexes can be notably spotted which might have also been affected due to the local environment, thus affecting the behaviour of ligands. In ligand-bound states derived from MD, we observe that ligand binding does not induce much changes to the surface charge distribution of the binding site of TREM2 ECD. Additionally, our hydrogen bond analysis using the *gmx hbond* utility of GROMACS is in concurrent with the intermolecular contact analysis (Fig. 4C). Thus, it can be suggested that TREM2 ECD interacts with its ligands mostly with hydrophobic contacts.

3.4. Ligand binding affects the structure of binding site I

Previously, studies have shown that over-expression of TREM2 leads to decrease in inducible nitric oxide synthase (iNOS) and proinflammatory cytokines expression level and thus inhibits microglia M1 polarization, while on the contrary increases the level of Arginase 1 (Arg1) and anti-inflammatory cytokine expression and enhances polarization of microglia M2. An in-depth analysis of microglia M1/M2 polarization suggests that microglia exists in multiple, dynamic and multidimensional states and are physiologically

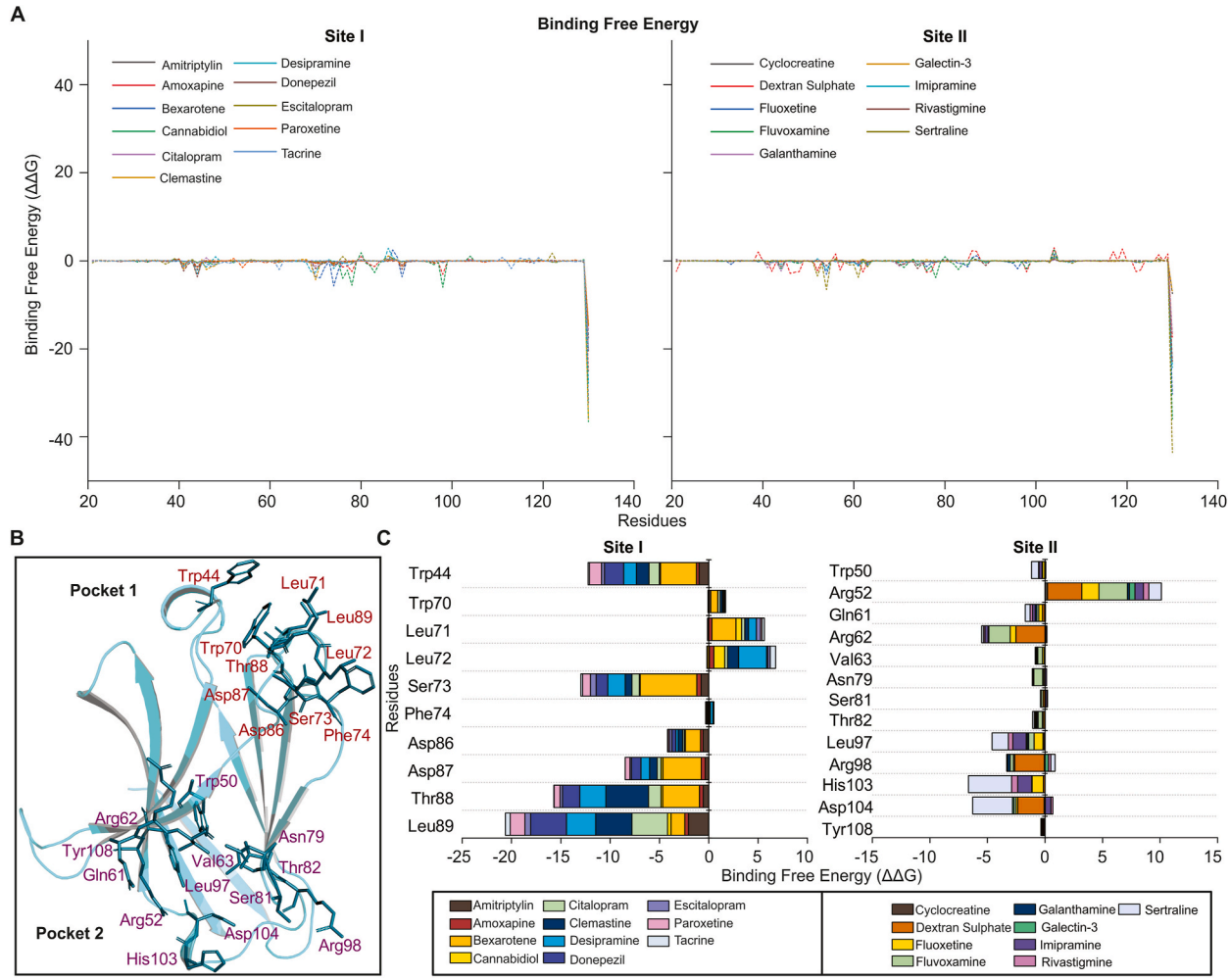

Fig. 7. Binding energy of each TREM2 ECD-ligand complexes calculated through MMPBSA approach. (**A**) Line plots indicating the total binding energy of each TREM2 ECD-ligand complexes for both site I and site II. (**B**) Key residues having maximum contribution towards the process of molecular recognition of TREM2 ligands. (**C**) Binding free energy decomposition analysis demonstrates the contribution of each key residue towards the recognition of each ligand by TREM2 ECD.

dependent on their environmental changes [80]. However, the process of TREM2 modulated microglia polarization and AD regulation requires further investigations [81]. In the context of these revelations, structural studies on TREM2 are required for exploring numerous unresolved questions underneath microglia functioning.

TREM2 CDR loops, i.e., CDR1 (residues Pro37 to Arg47), CDR2 (residues Thr66 to Arg76) and CDR3 (residues His114 and Glu117) are major complementarity determining regions. Among them, CDR2 loop has been shown to be critical for maintaining a stable conformation for ECD through a dense network of hydrogen bonds with CDR1 loop [62]. Moreover, both CDR1 and CDR2 are equally important for forming site I ligand binding site. Also, studies have shown that CDR2 loop remodels from an irregular conformation to a short helix upon R47H mutation [58]. Our computational investigation on the structural changes in ECD upon binding ligands through RMSF analyses reveals that β-strands B, C, D, F, CDR1 and CDR2 loops showed similar range of fluctuations which also aligns with the RMSF profile of apo TREM2 ECD (Figure S7 (A and B)). More specifically, maximum fluctuation in the CDR2 loop was observed in case of Bexarotene from site I and Galectin-3 from site II, which is similar to the one observed in the R47H mutant (Fig. S7C) and might affect the stability of TREM2-ECD. Thus, it can be inferred that CDR2 loop is often prone to conformational changes. On the contrary, higher and similar range of flexibility in loop connecting β-strands D and E and CDR3 loop was also evident in all the TREM2 ECD and ligand complexes (Fig. 5 and S6).

To further measure the range of flexibility of our key residues, we calculated their RMSF profiles, as illustrated in the bar plot in Fig. 5. As can be evident from the plot, we observe maximum fluctuation in residues from site I, with Trp70 and Leu71, while Asn79, His103 and Asp104 exhibiting maximum RMSF values in site II.

3.5. Principal component analysis

The most important elements such as atomic displacements in each ligand-bound conformation of TREM2 ECD from the MD trajectories were extracted using a covariance matrix from its atomic coordinates [82]. A set of orthogonal collective modes, known as eigenvectors or principal components with their corresponding eigenvalue, symbolizing motion of the atom were decomposed together to form a covariance-matrix. The larger motions of each principal component (PC) is usually stored in the larger eigenvalues [83]. Investigation of the initial PCs of MD trajectories thus provides us information regarding direction and region of motion in TREM2 ECD. Fig. S8 demonstrates the superposition of TREM2 ECD eigenvectors from the last 100 ns MD trajectories of each TREM2 ECD-ligand complexes. The trace values for site I binding ligand complexes Amitriptylin, Amoxapine, Bexarotene, Cannabidiol, Citalopram, Clemastine, Desipramine, Donepezil, Escitalopram, Paroxetine, and Tacrine was found to be 3.46, 3.30, 3.07, 4.04, 3.10, 3.81, 3.75, 3.04, 3.11, 3.52 and 3.34 nm^2 respectively. On the other hand, the trace values of site II binding ligand complexes Cyclocreatine, Detran Sulphate, Fluoxetine, Fluvoxamine, Galanthamine, Galectin-3, Imipramine, Rivastigmine and Sertraline were

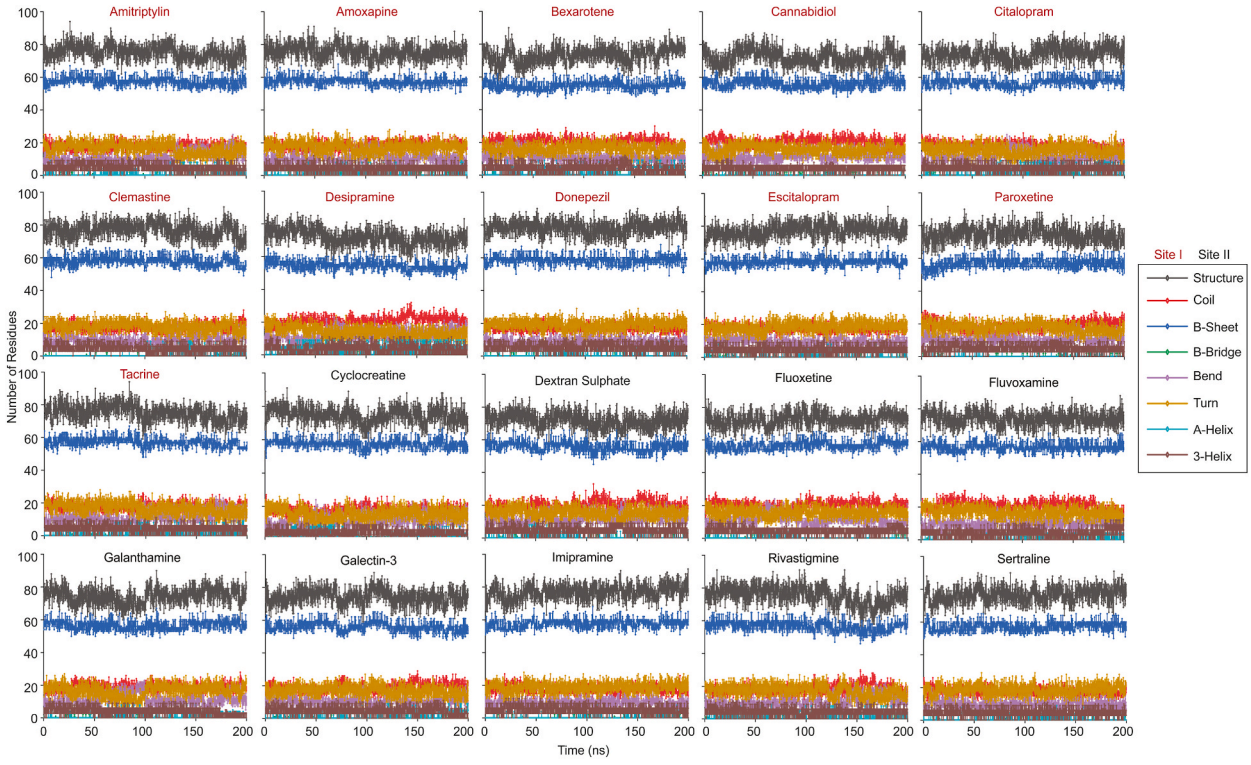

Fig. 8. Time step evolution of each secondary structural element of TREM2 ECD in all the twenty ligand bound TREM2 ECD complexes.

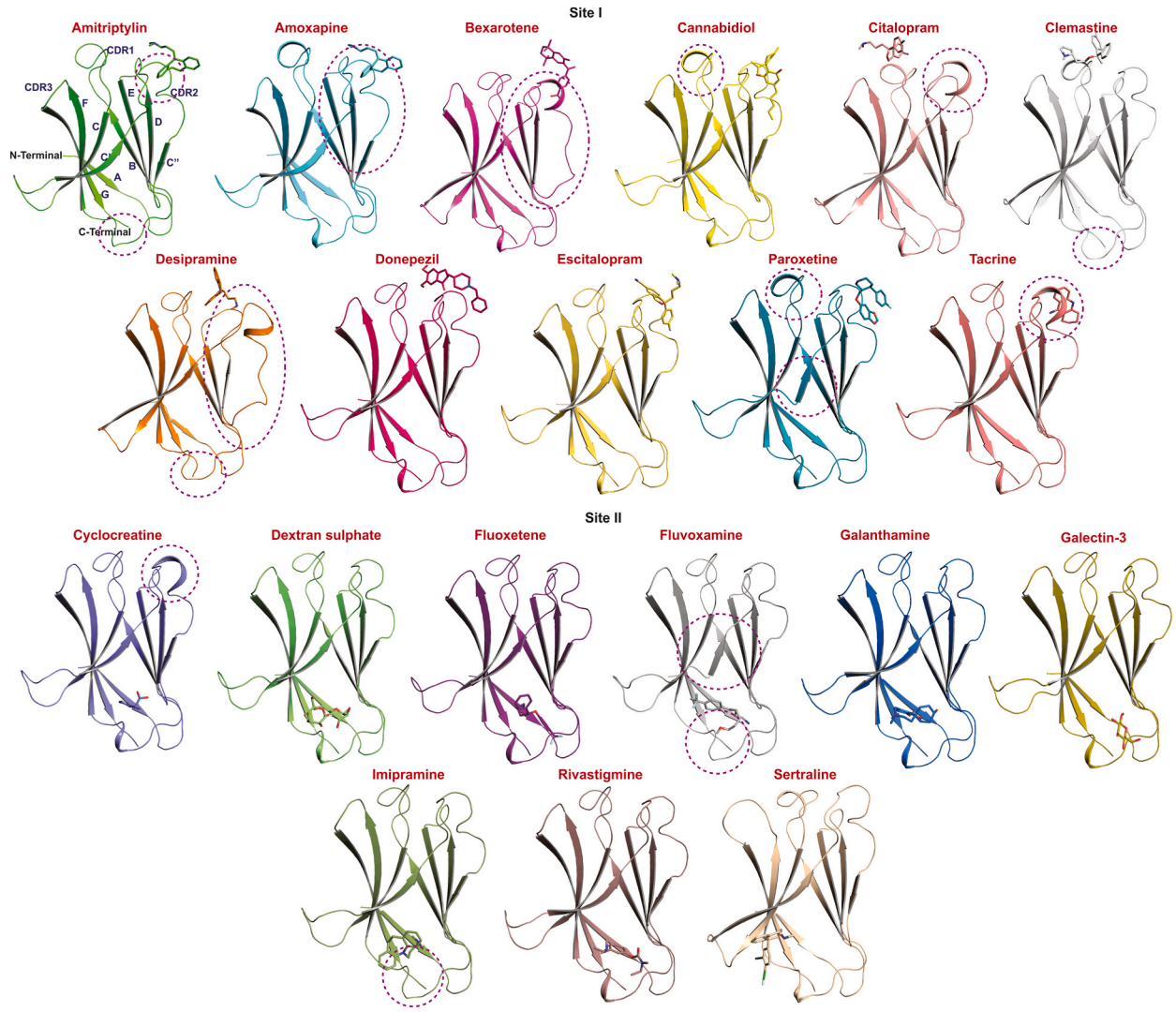

Fig. 9. Top ranked cluster representatives of the MD simulated TREM2 ECD-ligand complexes highlighting structural changes in TREM2 ECD upon binding to ligands. ECD regions undergoing structural changes have been highlighted through dotted circles.

observed to be 3.32, 3.48, 4.77, 3.29, 3.41, 4.77, 3.42, 4.51, 2.89 nm^2.

As can be evident from the porcupine plots, significant atomic movements were observed in case of CDR2 loop in Amitriptylin (only in PC1), Bexarotene, Cannabidiol, Clemastine, and Desipramine in both PC1 and PC2 (Fig. 6A and S9), and smaller movements in CDR3 loop were also observed in CDR3 loop of Amitriptylin. Also, the loop connecting β-strand C and C′ showed significant movements in all the site I binding ligand complexes, except for Paroxetine and Tacrine. Despite of the binding site, we observed a similar trend of atomic displacements in case of CDR2 loop in site II binding ligands such as Fluvoxamine and Galectine-3 in PC1 plots, while Sertraline in PC2 plot exhibited smaller outward movements. Moreover, in case of loop connecting β-strand C and C′ we observed outward movements in all the complexes in both PC1 and PC2 plots, except for Galectin-3, which showed some movements only in case of PC2 plots. Some large outward movement in β-strand B was also noticed in case of Rivastigmine (Fig. 6B and S9). On the other hand, the PC1 porcupine plot of apo TREM2 ECD, as demonstrated in Fig. S9B, small minimal movements were observed in CDR2 loop and loop connecting β-strand C and C'. Altogether, we have observed that Bexarotene and Galectin-3 binding to TREM2 ECD results in maximum movements in case of CDR2 loop, similar to that of the R47H mutant (Fig. S7D) which is in support of our RMSF analysis.

3.6. Prediction of binding free energies (ΔG_{bind}) using MM/PBSA approach

TREM2 has a widespread role in modulating AD by mediating numerous metabolic pathways in the microglia. Other than inducing microglia polarization, TREM2 has been seen to mediate the pathological range of phosphorylated Tau by microglia-Aβ interaction, which is again modulated by PI3K/AKT/GSK-3β signalling pathway [84]. However, TREM2 deficiency or loss of TREM2 function have

been observed to promote accumulation of pathological Tau in presence of Aβ plaques, decrease in microglia and increase in Aβ deposition [85–87]. Notably, loss of TREM2 functioning has also been observed to result in pathogenic lipid metabolism in microglia [88]. Mechanically, TREM2 can also promote microglia proliferation by activating Wnt/beta-catenin signalling pathway [56], microglia chemotaxis by activating focal adhesion kinase and FAK/Racl/Cdc42-GTPase signalling pathway [89] and also induces the phosphorylation of extracellular signal-regulated kinase to increase the expression of chemokine receptor 7 on the surface of microglia and promote microglia migration [90]. Other than that, TREM2 also plays significant role in microglia phagocytosis by altering inflammatory environment surrounding Aβ and also affects the lipid metabolism in microglia [91]. Thus, to contribute towards gaining insights into the specific roles of TREM2 in human brain or AD patients, we were focused on analysing the kind of interactions between TREM2 and its known ligands through calculating their binding free energies.

Binding free energies of any biomolecular complexes aids in determining the strength of their interactions. Amongst all the known approaches, MM-PBSA has surpassed as one of the most widely implemented methods to calculate the interaction energies between any two biomolecules by decomposing the total binding energy into a series of energetic components [92]. MM-PBSA approach implemented in MD simulated complexes is often used to re-score a set of docked complexes, improve its utility and generate an ensemble of binding conformations in the presence of explicit water [53]. The binding free energies of each TREM2 ECD-ligand complexes (Fig. 7A) attained using the MD simulated systems has been enlisted in Table S3. As can be evident from Table S3, van der Waals has the most contribution towards ΔG_{bind} which was also evident in our previous studies [54,76].

To further achieve insights into the contribution of each key residues towards the process of molecular recognition of TREM2 ligands, we performed the binding free energy decomposition analysis. Positional view of key residues in TREM2 ECD contributing towards binding free energy have been illustrated in Fig. 7B. Evidently, in case of site I binding ligand complexes, Trp44 (CDR1), Ser73 (CDR2), Thr88 and Leu89 (loop connecting β-strand D and E) were observed to have significant contribution towards the binding process, while Arg62 (β-strand C'), His103 and Asp104 (loop connecting β-strand E and F) had most contribution in case of site II binding ligand complexes (Fig. 7C).

3.7. Conformational changes in TREM2 ECD upon ligand binding

Major conformational changes in CDR2 loop such as development of a distinct and non-standard 2-turn helix have been observed by Sudom et al. which involves the alteration of pH dependence in Arg47 upon interaction with residue His67 [62]. This alteration in the conformation of CDR2 loop also leads to substantial changes in the putative positive ligand-interacting surface (PLIS), i.e. site I. Moreover, mutation of R47H was observed to reduce the stability of CDR2 loop and its downstream β-strand C" [62]. In concordance to the study by Sudom et al. another study has also revealed the difference in the stability and secondary structure of TREM2 ECD in both the WT and R47H mutant which has been hypothesized to be the effect of point mutation [93].

Evolution of secondary structures throughout the 200 ns timescale of MD simulations have been demonstrated in Fig. 8. The visual interpretation of changes in the secondary structure profile of TREM2 ECD as demonstrated in Fig. 9 has been achieved with the help of the top cluster representatives of each MD simulated complex. As can be evident from both the figures, some shift in the conformation of the secondary structure of TREM2 ECD can be observed throughout the 200 ns MD run. Moreover, major shift in the β-strand A can be evident in case of Paroxetine and Fluvoxamine. On the other hand, noticeable formation of a small helix in CDR2 loop was observed in case of Amoxapine, Cannabidiol, Clemastine and Paroxetine, similar to the one observed in case of R47H mutant (Fig. S10) [62]. Additionally, a development of small helix in CDR3 loop of Amoxapine, Cannabidiol, Clemastine and Paroxetine was also observed. Furthermore, loss of β-strand C" was an unusual event observed in case of Bexarotene and Desipramine. Also, loss of helicity in the loop connecting β-strand E and F was evident in case of amitriptyline, Clemastine, Desipramine, Fluvoxamine and Imipramine bound TREM2 ECD complexes. The superimposed view of all the TREM2 ECD-ligand complexes have been illustrated in Fig. S11. Altogether, it can be seen that, ligand binding mostly affects the PLIS or site I of TREM2 ECD.

4. Conclusion

TREM2 has been aggressively highlighted in numerous studies for its significant role in the progression of AD. Our study, while focusing on the active interaction between TREM2 ECD and its known ligands identifies multiple ligand binding sites.

Our extensive computational approach, as for our knowledge, for the first time reports the presence of site II ligand binding site in TREM2 ECD with the help of machine learning guided molecular docking. Further analyses of plasticity and essential dynamics of TREM2 ECD-ligand complexes emphasizes over the hypothesis that irrespective of the binding site, CDR2 is the most affected secondary structural element in TREM2 ECD, which is also supported by our secondary structural element analysis of the top cluster representatives.

Moreover, our MD study and free energy decomposition analysis identifies Trp44, Ser73, Thr88 and Leu89 from site I and Arg62, His103 and Asp104 residues from site II to be significantly involved in the process of molecular recognition of TREM2 ligands. However, our study is limited to only twenty known ligands of TREM2, investigation of other ligands might provide several other critical insights into ligand recognition process, which may open up new avenues for development of novel therapeutics against AD. Also, further experimental investigations are required to confirm our hypothesis.

In summary, our computational approach provides a great framework for understanding the molecular basis of interaction between TREM2 ECD and its known ligands, which can also aid in achieving more insights into the functioning of TREM2 signalling biology and its dysregulation in neurodegenerative diseases like AD.

CRediT authorship contribution statement

Sarbani Mishra: Writing – original draft, Software, Methodology, Formal analysis, Data curation. **Preety Sthutika Swain:** Writing – original draft, Methodology, Data curation. **Sanghamitra Pati:** Writing – review & editing, Visualization, Project administration. **Budheswar Dehury:** Writing – review & editing, Project administration, Investigation, Data curation, Conceptualization.

Data availability statement

Data will be made available on request. For requesting data, please write to the corresponding author.

Funding

This research received no external funding.

Declaration of competing interest

The authors declare that they have no known competing financial interests or personal relationships that could have appeared to influence the work reported in this paper.

Acknowledgments

The authors would like to acknowledge ICMR-Regional Medical Research Centre, Bhubaneswar for the computational facility to carry out the work. The authors also acknowledge Manipal School of Life Sciences, Manipal Academy of Higher Education, Manipal for providing necessary facilities to execute the work.

Appendix A. Supplementary data

Supplementary data to this article can be found online at https://doi.org/10.1016/j.heliyon.2024.e41414.

References

[1] M. Colonna, The biology of TREM receptors, Nat. Rev. Immunol. 23 (9) (2023) 580–594, https://doi.org/10.1038/s41577-023-00837-1.
[2] M. Colonna, Trems in the immune system and beyond, Nat. Rev. Immunol. 3 (6) (2003) 445–453, https://doi.org/10.1038/nri1106.
[3] A. Paradowska-Gorycka, M. Jurkowska, Structure, expression pattern and biological activity of molecular complex TREM-2/DAP12, Hum. Immunol. 74 (6) (2013) 730–737, https://doi.org/10.1016/j.humimm.2013.02.003.
[4] J. Walter, The triggering receptor expressed on myeloid cells 2: a Molecular link of neuroinflammation and neurodegenerative diseases, J. Biol. Chem. 291 (9) (2016) 4334–4341, https://doi.org/10.1074/jbc.R115.704981.
[5] M. Colonna, Y. Wang, TREM2 variants: new keys to decipher Alzheimer disease pathogenesis, Nat. Rev. Neurosci. 17 (4) (2016) 201–207, https://doi.org/10.1038/nrn.2016.7.
[6] R. Guerreiro, et al., TREM2 variants in Alzheimer's disease, N. Engl. J. Med. 368 (2) (2013) 117–127, https://doi.org/10.1056/nejmoa1211851.
[7] T. Jonsson, et al., Variant of TREM2 associated with the risk of Alzheimer's disease, N. Engl. J. Med. 368 (2) (2013) 107–116.
[8] S. Rayaprolu, et al., TREM2 in neurodegeneration: evidence for association of the p.R47H variant with frontotemporal dementia and Parkinson's disease, Mol. Neurodegener. 8 (1) (2013) 1, https://doi.org/10.1186/1750-1326-8-19.
[9] B. Borroni, et al., Heterozygous TREM2 mutations in frontotemporal dementia, Neurobiol. Aging 35 (4) (2014), https://doi.org/10.1016/j.neurobiolaging.2013.09.017, 934.e7-934.e10.
[10] E. Cuyvers, et al., Investigating the role of rare heterozygous TREM2 variants in Alzheimer's disease and frontotemporal dementia, Neurobiol. Aging 35 (3) (2014) 726.e11–726.e19, https://doi.org/10.1016/j.neurobiolaging.2013.09.009.
[11] Y. Fu, J. Zhao, Z. Chen, Insights into the molecular mechanisms of protein-ligand interactions by molecular docking and molecular dynamics simulation: a case of oligopeptide binding protein, Comput. Math. Methods Med. 2018 (2018), https://doi.org/10.1155/2018/3502514.
[12] Y. Atagi, et al., Apolipoprotein E is a ligand for triggering receptor expressed on myeloid cells 2 (TREM2), J. Biol. Chem. 290 (43) (2015) 26043–26050, https://doi.org/10.1074/jbc.M115.679043.
[13] C.C. Bailey, L.B. Devaux, M. Farzan, The triggering receptor expressed on myeloid cells 2 binds apolipoprotein E, J. Biol. Chem. 290 (43) (2015) 26033–26042, https://doi.org/10.1074/jbc.M115.677286.
[14] W. Y., TREM2 lipid sensing sustains the microglial response in an Alzheimer's disease model, Cell 160 (6) (2015) 1061–1071.
[15] F.L. Yeh, Y. Wang, I. Tom, L.C. Gonzalez, M. Sheng, TREM2 binds to apolipoproteins, including APOE and CLU/APOJ, and thereby facilitates uptake of amyloid-beta by microglia, Neuron 91 (2) (2016) 328–340, https://doi.org/10.1016/j.neuron.2016.06.015.
[16] D.L. Kober, T.J. Brett, TREM2-Ligand interactions in health and disease, J. Mol. Biol. 429 (11) (2017) 1607–1629, https://doi.org/10.1016/j.jmb.2017.04.004.
[17] C.B. Read, et al., Cutting edge: identification of neutrophil PGLYRP1 as a ligand for TREM-1, J. Immunol. 194 (4) (2015) 1417–1421, https://doi.org/10.4049/jimmunol.1402303.
[18] Q. Peng, S. Malhotra, J.A. Torchia, W.G. Kerr, K.M. Coggeshall, M.B. Humphrey, TREM2- and DAP12-dependent activation of PI3K requires DAP10 and is inhibited by SHIP1, Sci. Signal. 3 (122) (2010), https://doi.org/10.1126/scisignal.2000500.
[19] P. Wunderlich, K. Glebov, N. Kemmerling, N.T. Tien, H. Neumann, J. Walter, Sequential proteolytic processing of the triggering receptor expressed on myeloid cells-2 (TREM2) protein by ectodomain shedding and γ-secretase- dependent intramembranous cleavage, J. Biol. Chem. 288 (46) (2013) 33027–33036, https://doi.org/10.1074/jbc.M113.517540.
[20] D. Feuerbach, et al., ADAM17 is the main sheddase for the generation of human triggering receptor expressed in myeloid cells (hTREM2) ectodomain and cleaves TREM2 after Histidine 157, Neurosci. Lett. 660 (2017) 109–114, https://doi.org/10.1016/j.neulet.2017.09.034.

[21] C.L. Hsieh, et al., A role for TREM2 ligands in the phagocytosis of apoptotic neuronal cells by microglia, J. Neurochem. 109 (4) (2009) 1144–1156, https://doi.org/10.1111/j.1471-4159.2009.06042.x.

[22] C.B. Lessard, et al., " High-affinity interactions and signal transduction between Aβ oligomers and TREM 2 ,", EMBO Mol. Med. 10 (11) (2018) 1–13, https://doi.org/10.15252/emmm.201809027.

[23] F. Filipello, et al., The microglial innate immune receptor TREM2 is required for synapse elimination and normal brain connectivity, Immunity 48 (5) (2018) 979–991.e8, https://doi.org/10.1016/j.immuni.2018.04.016.

[24] K. Takahashi, C.D.P. Rochford, H. Neumann, Clearance of apoptotic neurons without inflammation by microglial triggering receptor expressed on myeloid cells-2, J. Exp. Med. 201 (4) (2005) 647–657, https://doi.org/10.1084/jem.20041611.

[25] G. Kleinberger, et al., " the FTD -like syndrome causing TREM 2 T66M mutation impairs microglia function, brain perfusion, and glucose metabolism ,", EMBO J. 36 (13) (2017) 1837–1853, https://doi.org/10.15252/embj.201796516.

[26] T. Xue, et al., Sphingosine-1-phosphate, a novel TREM2 ligand, promotes microglial phagocytosis to protect against ischemic brain injury, Acta Pharm. Sin. B 12 (4) (2022) 1885–1898, https://doi.org/10.1016/j.apsb.2021.10.012.

[27] S. Spiegel, S. Milstien, The outs and the ins of sphingosine-1-phosphate in immunity, Nat. Rev. Immunol. 11 (6) (2011) 403–415, https://doi.org/10.1038/nri2974.

[28] B. Luo, et al., Erythropoeitin signaling in macrophages promotes dying cell clearance and immune tolerance, Immunity 44 (2) (2016) 287–302, https://doi.org/10.1016/j.immuni.2016.01.002.

[29] T. H.B., Disrupted epithelial/macrophage crosstalk via Spinster homologue 2-mediated S1P signaling may drive defective macrophage phagocytic function in COPD, PLoS One 12 (11) (2017) e0179577.

[30] M. Hutton, J. Pérez-Tur, J. Hardy, Genetics of Alzheimer's disease, Essays Biochem. 33 (1998) 117–131, https://doi.org/10.1042/bse0330117.

[31] G. Kleinberger, et al., TREM2 mutations implicated in neurodegeneration impair cell surface transport and phagocytosis, Sci. Transl. Med. 6 (243) (2014), https://doi.org/10.1126/scitranslmed.3009093.

[32] C. Condello, P. Yuan, J. Grutzendler, Microglia-mediated neuroprotection, TREM2, and Alzheimer's disease: evidence from optical imaging, Biol. Psychiatry 83 (4) (2018) 377–387, https://doi.org/10.1016/j.biopsych.2017.10.007.

[33] J.S. Park, I.J. Ji, D.H. Kim, H.J. An, S.Y. Yoon, The Alzheimer's disease-associated R47H variant of TREM2 has an altered glycosylation pattern and protein stability, Front. Neurosci. 10 (JAN) (2017), https://doi.org/10.3389/fnins.2016.00618.

[34] X. Wu, L.Y. Xu, E.M. Li, G. Dong, Application of molecular dynamics simulation in biomedicine, Chem. Biol. Drug Des. 99 (5) (2022) 789–800, https://doi.org/10.1111/cbdd.14038.

[35] P.E.B.H.M. Berman, J. Westbrook, Z. Feng, G. Gilliland, T.N. Bhat, H. Weissig, I.N. Shindyalov, H.M. Berman, J. Westbrook, Z. Feng, G. Gilliland, T.N. Bhat, H. Weissig, I.N. Shindyalov, P.E. Bourne, The protein data bank nucleic acids research, 28: 235-242, Protein Data Bank Nucleic Acids Res 28 (2000) 235–242, 2000.

[36] S. Kim, et al., PubChem 2023 update, Nucleic Acids Res. 51 (D1) (2023) D1373–D1380, https://doi.org/10.1093/nar/gkac956.

[37] A.D. Hunter, ACD/ChemSketch 1.0 (freeware); ACD/ChemSketch 2.0 and its tautomers, dictionary, and 3D plug-ins; ACD/HNMR 2.0; ACD/CNMR 2.0, J. Chem. Educ. 74 (8) (1997) 905, https://doi.org/10.1021/ed074p905.

[38] J. Eberhardt, D. Santos-Martins, A.F. Tillack, S. Forli, AutoDock Vina 1.2.0: new docking methods, expanded force field, and Python bindings, J. Chem. Inf. Model. 61 (8) (2021) 3891–3898, https://doi.org/10.1021/acs.jcim.1c00203.

[39] N.M. O'Boyle, M. Banck, C.A. James, C. Morley, T. Vandermeersch, G.R. Hutchison, Open Babel: an open chemical toolbox, J. Cheminform. 3 (10) (2011), https://doi.org/10.1186/1758-2946-3-33.

[40] Z. Wang, et al., Comprehensive evaluation of ten docking programs on a diverse set of protein-ligand complexes: the prediction accuracy of sampling power and scoring power, Phys. Chem. Chem. Phys. 18 (18) (2016) 12964–12975, https://doi.org/10.1039/c6cp01555g.

[41] O. Trott, A.J. Olson, AutoDock Vina: improving the speed and accuracy of docking with a new scoring function, efficient optimization, and multithreading, J. Comput. Chem. 31 (2) (2010) 455–461, https://doi.org/10.1002/jcc.21334.

[42] S.S. Swain, et al., Molecular docking and simulation study for synthesis of alternative dapsone derivative as a newer antileprosy drug in multidrug therapy, J. Cell. Biochem. 119 (12) (2018) 9838–9852, https://doi.org/10.1002/jcb.27304.

[43] S. Mishra, M. Rout, M.K. Singh, B. Dehury, S. Pati, Classical molecular dynamics simulation identifies catechin gallate as a promising antiviral polyphenol against MPOX palmitoylated surface protein, Comput. Biol. Chem. (2024) 108070, https://doi.org/10.1016/j.compbiolchem.2024.108070.

[44] J. Huang, et al., CHARMM36m: an improved force field for folded and intrinsically disordered proteins, Nat. Methods 14 (1) (2016) 71–73, https://doi.org/10.1038/nmeth.4067.

[45] K. Vanommeslaeghe, A.D. MacKerell, Automation of the CHARMM general force field (CGenFF) I: bond perception and atom typing, J. Chem. Inf. Model. 52 (12) (2012) 3144–3154, https://doi.org/10.1021/ci300363c.

[46] M. Parrinello, A. Rahman, Polymorphic transitions in single crystals: a new molecular dynamics method, J. Appl. Phys. 52 (12) (1981) 7182–7190, https://doi.org/10.1063/1.328693.

[47] W.G. Hoover, Canonical dynamics: equilibrium phase-space distributions, Phys. Rev. A 31 (3) (1985) 1695–1697, https://doi.org/10.1103/PhysRevA.31.1695.

[48] T. Darden, D. York, L. Pedersen, Particle mesh Ewald: an N·log(N) method for Ewald sums in large systems, J. Chem. Phys. 98 (12) (1993) 10089–10092, https://doi.org/10.1063/1.464397.

[49] V. Kräutler, W.F. Van Gunsteren, P.H. Hünenberger, A fast SHAKE algorithm to solve distance constraint equations for small molecules in molecular dynamics simulations, J. Comput. Chem. 22 (5) (2001) 501–508, https://doi.org/10.1002/1096-987X(20010415)22:5<501::AID-JCC1021>3.0.CO;2-V.

[50] B. Dehury, K.P. Kepp, Membrane dynamics of γ-secretase with the anterior pharynx-defective 1B subunit, J. Cell. Biochem. 122 (1) (2021) 69–85, https://doi.org/10.1002/jcb.29832.

[51] B. Dehury, N. Tang, K.P. Kepp, Molecular dynamics of C99-bound γ-secretase reveal two binding modes with distinct compactness, stability, and active-site retention: implications for Aβ production, Biochem. J. 476 (7) (2019) 1173–1189, https://doi.org/10.1042/BCJ20190023.

[52] B. Dehury, S.K. Behera, N. Mahapatra, Structural dynamics of Casein Kinase I (CKI) from malarial parasite Plasmodium falciparum (Isolate 3D7): insights from theoretical modelling and molecular simulations, J. Mol. Graph. Model. 71 (2017) 154–166, https://doi.org/10.1016/j.jmgm.2016.11.012.

[53] R. Kumari, R. Kumar, A. Lynn, G-mmpbsa -A GROMACS tool for high-throughput MM-PBSA calculations, J. Chem. Inf. Model. 54 (7) (2014) 1951–1962, https://doi.org/10.1021/ci500020m.

[54] S. Mishra, M. Rout, M. Kumar, Illuminating the Structural Basis of Human Neurokinin 1 Receptor (NK1R) Antagonism through Classical All - Atoms Molecular Dynamics Simulations, September, 2023, https://doi.org/10.1002/jcb.30493.

[55] T. Jonsson, et al., " variant of TREM2 associated with the risk of Alzheimer's disease ,", N. Engl. J. Med. 368 (2) (2013) 107–116, https://doi.org/10.1056/nejmoa1211103.

[56] W.C. Carlyle, et al., TREM2 maintains microglial metabolic fitness in Alzheimer's disease, Cell 162 (3) (2015) 561–567.

[57] X.-Y. Meng, H.-X. Zhang, M. Mezei, M. Cui, Molecular docking: a powerful approach for structure-based drug Discovery, Curr. Comput. Aided Drug Des. 7 (2) (2012) 146–157, https://doi.org/10.2174/157340911795677602.

[58] A. Sudom, et al., Molecular basis for the loss-of-function effects of the Alzheimer's disease–associated R47H variant of the immune receptor TREM2, J. Biol. Chem. 293 (32) (2018) 12634–12646, https://doi.org/10.1074/jbc.ra118.002352.

[59] L. Jendele, R. Krivak, P. Skoda, M. Novotny, D. Hoksza, PrankWeb: a web server for ligand binding site prediction and visualization, Nucleic Acids Res. 47 (W1) (2019) W345–W349, https://doi.org/10.1093/nar/gkz424.

[60] A.F. Williams, A.N. Barclay, The immunoglobulin superfamily - domains for cell surface recognition, Annu. Rev. Immunol. 6 (1988) 381–405, https://doi.org/10.1146/annurev.iy.06.040188.002121.

[61] R. Dash, H.J. Choi, I.S. Moon, Mechanistic insights into the deleterious roles of Nasu-Hakola disease associated TREM2 variants, Sci. Rep. 10 (1) (2020), https://doi.org/10.1038/s41598-020-60561-x.

[62] A. Sudom, et al., Molecular basis for the loss-of-function effects of the Alzheimer's disease–associated R47H variant of the immune receptor TREM2, J. Biol. Chem. 293 (32) (2018) 12634–12646, https://doi.org/10.1074/jbc.ra118.002352.
[63] D.L. Kober, et al., Functional insights from biophysical study of TREM2 interactions with apoE and Aβ1-42, Alzheimer's Dement. 17 (3) (2021) 475–488, https://doi.org/10.1002/alz.12194.
[64] S. Mishra, M. Rout, N.L. Simha, B. Dehury, S. Pati, Insights into lipid-modified recognition of Apolipoprotein E3 to extra-cellular domain of TREM2 associated with Alzheimer's disease, J. Mol. Liq. 415 (PA) (2024) 126281, https://doi.org/10.1016/j.molliq.2024.126281.
[65] J.A. Greven, et al., Biophysical mapping of TREM2-ligand interactions reveals shared surfaces for engagement of multiple Alzheimer's disease ligands, Res. Sq. (2024), https://doi.org/10.21203/rs.3.rs-4850141/v1.
[66] V. Zerbi, et al., Brain mapping across 16 autism mouse models reveals a spectrum of functional connectivity subtypes, Mol. Psychiatry 26 (12) (2021) 7610–7620, https://doi.org/10.1038/s41380-021-01245-4.
[67] E. Tagliatti, et al., Trem2 expression in microglia is required to maintain normal neuronal bioenergetics during development, Immunity 57 (1) (2024) 86–105. e9, https://doi.org/10.1016/j.immuni.2023.12.002.
[68] J. Cheng, et al., Early glycolytic reprogramming controls microglial inflammatory activation, J. Neuroinflammation 18 (1) (2021), https://doi.org/10.1186/s12974-021-02187-y.
[69] R. Holland, et al., Inflammatory microglia are glycolytic and iron retentive and typify the microglia in APP/PS1 mice, Brain Behav. Immun. 68 (2018) 183–196, https://doi.org/10.1016/j.bbi.2017.10.017.
[70] C. Lauro, C. Limatola, Metabolic reprograming of microglia in the regulation of the innate inflammatory response, Front. Immunol. 11 (2020), https://doi.org/10.3389/fimmu.2020.00493.
[71] A. Deczkowska, H. Keren-Shaul, A. Weiner, M. Colonna, M. Schwartz, I. Amit, Disease-associated microglia: a universal immune sensor of neurodegeneration, Cell 173 (5) (2018) 1073–1081, https://doi.org/10.1016/j.cell.2018.05.003.
[72] A.M. Szczepanik, S. Funes, W. Petko, G.E. Ringheim, IL-4, IL-10 and IL-13 modulate Aβ(1-42)-induced cytokine and chemokine production in primary murine microglia and a human monocyte cell line, J. Neuroimmunol. 113 (1) (2001) 49–62, https://doi.org/10.1016/S0165-5728(00)00404-5.
[73] K. Kawahara, et al., Intracerebral microinjection of interleukin-4/interleukin-13 reduces β-amyloid accumulation in the ipsilateral side and improves cognitive deficits in young amyloid precursor protein 23 mice, Neuroscience 207 (2012) 243–260, https://doi.org/10.1016/j.neuroscience.2012.01.049.
[74] O. Berezovska, M.Q. Xia, B.T. Hyman, Notch is expressed in adult brain, is coexpressed with presenilin-1, and is altered in Alzheimer disease, J. Neuropathol. Exp. Neurol. 57 (8) (1998) 738–745, https://doi.org/10.1097/00005072-199808000-00003.
[75] K. Schlepckow, et al., " Enhancing protective microglial activities with a dual function TREM 2 antibody to the stalk region ,", EMBO Mol. Med. 12 (4) (2020) https://doi.org/10.15252/emmm.201911227.
[76] M. Rout, S. Mishra, S. Dey, M.K. Singh, B. Dehury, S. Pati, Exploiting the potential of natural polyphenols as antivirals against monkeypox envelope protein F13 using machine learning and all-atoms MD simulations, Comput. Biol. Med. 162 (2023), https://doi.org/10.1016/j.compbiomed.2023.107116.
[77] M. Rout, et al., Machine learning and classical MD simulation to identify inhibitors against the P37 envelope protein of monkeypox virus, J. Biomol. Struct. Dyn. (2023), https://doi.org/10.1080/07391102.2023.2216290.
[78] J. Penney, et al., iPSC-derived microglia carrying the TREM2 R47H/+ mutation are proinflammatory and promote synapse loss, Glia 72 (2) (2024) 452–469, https://doi.org/10.1002/glia.24485.
[79] E. Dardiotis, et al., A novel mutation in TREM2 gene causing Nasu-Hakola disease and review of the literature, Neurobiol. Aging 53 (2017) 194.e13–194.e22, https://doi.org/10.1016/j.neurobiolaging.2017.01.015.
[80] J. Wang, W. He, J. Zhang, A richer and more diverse future for microglia phenotypes, Heliyon 9 (4) (2023) e14713, https://doi.org/10.1016/j.heliyon.2023.e14713.
[81] Q. Wang, Q. Wang, W. Yang, J. Zhang, Y. Zhao, Y. Xu, TREM2 overexpression attenuates cognitive deficits in experimental models of vascular dementia, Neural Plast. 2020 (2020), https://doi.org/10.1155/2020/8834275.
[82] M.A. Balsera, W. Wriggers, Y. Oono, K. Schulten, Principal component analysis and long time protein dynamics, J. Phys. Chem. 100 (7) (1996) 2567–2572, https://doi.org/10.1021/jp9536920.
[83] C.C. David, D.J. Jacobs, Principal component analysis: a method for determining the essential dynamics of proteins, Methods Mol. Biol. 1084 (2014) 193–226, https://doi.org/10.1007/978-1-62703-658-0_11.
[84] X. Peng, et al., TREM2 inhibits Tau hyperphosphorylation and neuronal apoptosis via the PI3K/Akt/GSK-3β signaling pathway in vivo and in vitro, Mol. Neurobiol. 60 (5) (2023) 2470–2485, https://doi.org/10.1007/s12035-023-03217-x.
[85] T.R. Jay, et al., TREM2 deficiency eliminates TREM2+ inflammatory macrophages and ameliorates pathology in Alzheimer's disease mouse models, J. Exp. Med. 212 (3) (2015) 287–295, https://doi.org/10.1084/jem.20142322.
[86] P. Yuan, et al., TREM2 haplodeficiency in mice and humans impairs the microglia barrier function leading to decreased amyloid compaction and severe axonal dystrophy, Neuron 90 (4) (2016) 724–739, https://doi.org/10.1016/j.neuron.2016.05.003.
[87] S.N. Rai, V.K. Chaturvedi, B.K. Singh, M.P. Singh, Commentary: trem2 deletion reduces late-stage amyloid plaque accumulation, elevates the Aβ42:Aβ40 ratio, and exacerbates axonal dystrophy and dendritic spine loss in the PS2APP Alzheimer's mouse model, Front. Aging Neurosci. 12 (2020), https://doi.org/10.3389/fnagi.2020.00219.
[88] G. Gouna, et al., TREM2-dependent lipid droplet biogenesis in phagocytes is required for remyelination, J. Exp. Med. 218 (10) (2021) e20210227, https://doi.org/10.1084/jem.20210227.
[89] Z. Rong, et al., Activation of FAK/Rac1/Cdc42-GTPase signaling ameliorates impaired microglial migration response to Aβ42 in triggering receptor expressed on myeloid cells 2 loss-of-function murine models, FASEB J 34 (8) (2020) 10984–10997, https://doi.org/10.1096/fj.202000550RR.
[90] C. Mecca, I. Giambanco, R. Donato, C. Arcuri, Microglia and aging: the role of the TREM2–DAP12 and CX3CL1-CX3CR1 Axes, Int. J. Mol. Sci. 19 (1) (2018), https://doi.org/10.3390/ijms19010318.
[91] K.M. Schoch, et al., Acute Trem2 reduction triggers increased microglial phagocytosis, slowing amyloid deposition in mice, Proc. Natl. Acad. Sci. U. S. A. 118 (27) (2021), https://doi.org/10.1073/pnas.2100356118.
[92] N. Homeyer, H. Gohlke, Free energy calculations by the molecular mechanics Poisson-Boltzmann surface area method, Mol. Inform. 31 (2) (2012) 114–122, https://doi.org/10.1002/minf.201100135.
[93] D.L. Kober, et al., Neurodegenerative disease mutations in TREM2 reveal a functional surface and distinct loss-of-function mechanisms, Elife 5 (2016) DECEMBER2016, https://doi.org/10.7554/eLife.20391.